Progress In Electromagnetics Research, PIER 57, 311–333, 2006

APPLYING DIVERGENCE-FREE CONDITION IN SOLVING THE VOLUME INTEGRAL EQUATION

M.-K. Li and W. C. Chew

Center of Computational Electromagnetics and
Electromagnetics Laboratory
University of Illinois at Urbana-Champaign
Urbana, IL, USA

Abstract—Applying divergence-free condition to volume integral equation solver will be discussed. Three schemes are available: basis reduction scheme, minimal complete volume loop basis set and expanded volume loop basis set. All of them will generate smaller matrix equations than the SWG basis. The first two schemes generate poorly-conditioned matrices that are hard to solve by iterative solvers. The expanded loop basis set is easier to solve iteratively in spite of the existence of a null space in the matrix. Moreover, the construction of the expanded loop basis set is much easier than the other two schemes.

1. INTRODUCTION

The volume integral equation (VIE) was first introduced by Esmarch [1] derived from the volume equivalence principle [2]. By the efforts of many researchers, this scheme has been successfully applied to numerically solve electromagnetic problems using the method of moments [3–5]. In these schemes, the dielectric object is discretized into sub-domains, and the electromagnetic parameters in each sub-domain are approximated by one unknown scalar multiplied by a known vector function called the basis function. Evaluating the interactions between these basis functions will lead to a matrix equation. The unknown scalars can be solved from this matrix equation as an approximation of the electric or magnetic field in the object.

Among the basis sets used in three-dimensional VIE solvers, the tetrahedral basis (SWG basis as named by the initials of the authors) defined by Schaubert, Wilton and Glisson [3] is one of the most widely used. It is suitable for modeling the electric current or electric flux in a dielectric scatterer by keeping the normal continuity

of the current or flux. However, the divergence of the SWG basis is not zero, which does not reflect the physics of the flux inside the scatterer. The authors reported that the divergence-free condition would be restored automatically by the integral equation, i.e., as the mesh density increases, the divergence of the electric flux inside each tetrahedron would converge to zero.

To apply the divergence-free condition directly to the VIE, Rubin [6] proposed a divergence-free basis to model the equivalent current flow in the dielectrics. Not only does this method apply the divergence free condition to the matrix equation, but also reduces the number of unknowns. However, this basis set is based on layered-surface mesh approximation of a volume.

The second method for applying the divergence-free condition is to use a loop basis set, which is inherently solenoidal. The loop basis generated from surface mesh has been studied and successfully applied to solve low frequency problems [7–11]. For volume tetrahedral mesh, Mendes and Carvalho proposed the volume solenoidal loop basis function [12, 13], which is an extension of the surface loop basis. Kulkarni et al. [14] analyzed this basis and called it edge basis because the basis functions were defined with respect to the edges in the geometrical mesh. From their results, the errors were smaller and the number of unknowns was also reduced using volume loop basis compared with the SWG basis. Although this conclusion was promising, one of the difficulties in the volume loop basis is in finding the minimum complete set of independent basis. The loop basis functions defined associated with every edge will not be independent of each other. Mendes and Kulkarni both noticed this problem. To address the problem, Mendes used Gram-Schmidt orthogonalization in [12, 13]; Kulkarni applied Gaussian elimination in [14] to select the independent basis set. The computational complexity of these two methods is large, and the physics is hidden in the computation of matrices. Therefore, a more efficient, physical method is needed to construct the independent loop basis set.

Although it is also possible to construct the independent loop basis set from a tetrahedral mesh by graph theory, the poor conditioning of the pertinent matrix equation restricts the use of iterative solvers such as the conjugate-gradient (CG) method.

In this paper, both the basis reduction scheme and the three-dimensional volume loop basis will be analyzed. A search algorithm for reduced basis and a more efficient search algorithm based on graph theory for the independent loop basis will be reported. Moreover, the speed of convergence to iteratively solve the matrix equations constructed from these two schemes will be analyzed. To improve

the convergence, an expanded volume loop basis set is proposed. The expanded volume loop basis set is easier to construct and also improves the convergence of the iterative solvers.

2. VOLUME INTEGRAL EQUATION

Assuming the permeability of the total space is a constant μ_b, VIE can be written as

$$\boldsymbol{E}^{inc}(\boldsymbol{r}) = \boldsymbol{E}(\boldsymbol{r}) - \omega^2\mu_b \int_V d\boldsymbol{r}' \overline{\boldsymbol{G}}(\boldsymbol{r},\boldsymbol{r}') \cdot [\varepsilon(\boldsymbol{r}') - \varepsilon_b]\boldsymbol{E}(\boldsymbol{r}') \tag{1}$$

where $\overline{\boldsymbol{G}}(\boldsymbol{r},\boldsymbol{r}')$ is the dyadic Green's function. The electric field can be solved from Eq. (1). This equation uses the E formulation. It can also be written into the J formulation by defining the current [3],

$$\boldsymbol{J}(\boldsymbol{r}) = -i\omega[\varepsilon(\boldsymbol{r}) - \varepsilon_b]\boldsymbol{E}(\boldsymbol{r}) \tag{2}$$

VIE can then be expressed as

$$\begin{aligned} -i\omega[\varepsilon(\boldsymbol{r}) - \varepsilon_b]\boldsymbol{E}^{inc}(\boldsymbol{r}) = & -i\omega[\varepsilon(\boldsymbol{r}) - \varepsilon_b]\boldsymbol{E}(\boldsymbol{r}) \\ & -\omega^2[\varepsilon(\boldsymbol{r}) - \varepsilon_b]\mu_b \int_V d\boldsymbol{r}' \overline{\boldsymbol{G}}(\boldsymbol{r},\boldsymbol{r}') \cdot \boldsymbol{J}(\boldsymbol{r}') \end{aligned} \tag{3}$$

i.e.,

$$\boldsymbol{J}^{inc}(\boldsymbol{r}) = \boldsymbol{J}(\boldsymbol{r}) - \omega^2[\varepsilon(\boldsymbol{r}) - \varepsilon_b]\mu_b \int_V d\boldsymbol{r}' \overline{\boldsymbol{G}}(\boldsymbol{r},\boldsymbol{r}') \cdot \boldsymbol{J}(\boldsymbol{r}') \tag{4}$$

VIE can also be written in the D formulation [15] in which the electric flux $\boldsymbol{D}(\boldsymbol{r})$ is used as the unknown, i.e.,

$$\boldsymbol{D}^{inc}(\boldsymbol{r}) = \frac{\varepsilon_b}{\varepsilon(\boldsymbol{r})}\boldsymbol{D}(\boldsymbol{r}) - \omega^2\mu_b \int_V d\boldsymbol{r}' \overline{\boldsymbol{G}}(\boldsymbol{r},\boldsymbol{r}') \cdot \frac{\varepsilon(\boldsymbol{r}) - \varepsilon_b}{\varepsilon(\boldsymbol{r})}\boldsymbol{D}(\boldsymbol{r}) \tag{5}$$

Eqs. (1), (4) and (5) are all based on the same principle and Green's function. They are different only in the unknown variable.

To solve either of the the above VIEs using the method of moments, the scatterer will be discretized into sub-domains, e.g., tetrahedrons. Basis functions are then defined associated with these sub-domains. The field or current at each point inside the scatterer can be approximated as a linear superposition of those basis functions. For example, the electric flux is discretized as

$$\boldsymbol{D}(\boldsymbol{r}) = \sum_{i=1}^{N} D_i \boldsymbol{f}_i(\boldsymbol{r}) \tag{6}$$

where $\boldsymbol{f}_i(\boldsymbol{r})$ is the i-th basis function, D_i is the coefficient describing the amplitude of the flux projected onto basis $\boldsymbol{f}_i$. With Eq. (6), the integral equation Eq. (5) can be transformed into a matrix equation:

$$\begin{aligned}\left\langle \boldsymbol{f}_i(\boldsymbol{r}), \boldsymbol{D}^{inc}(\boldsymbol{r})\right\rangle &= \sum_{j=1}^{N} D_j \left[\left\langle \boldsymbol{f}_i(\boldsymbol{r}), \frac{\varepsilon_b}{\varepsilon(\boldsymbol{r})}, \boldsymbol{f}_i(\boldsymbol{r})\right\rangle \right.\\ &\quad \left. - \omega^2\mu_b \left\langle \boldsymbol{f}_i(\boldsymbol{r}), \overline{\boldsymbol{G}}(\boldsymbol{r},\boldsymbol{r}')\frac{\varepsilon(\boldsymbol{r}')-\varepsilon_b}{\varepsilon(\boldsymbol{r}')}, \boldsymbol{f}_j(\boldsymbol{r}')\right\rangle\right]\\ &= \sum_{j=1}^{N} Z_{ij} D_j \end{aligned} \tag{7}$$

The field distribution can be achieved after solving this matrix equation. Furthermore, VIE can be derived from a variational form

$$\begin{aligned} I &= \langle \boldsymbol{D}(\boldsymbol{r}), \mathcal{L}(\boldsymbol{r},\boldsymbol{r}'), \boldsymbol{D}(\boldsymbol{r}')\rangle - 2\left\langle \boldsymbol{D}(\boldsymbol{r}), \frac{\xi(\boldsymbol{r})}{\varepsilon(\boldsymbol{r})}\boldsymbol{D}^{inc}(\boldsymbol{r})\right\rangle\\ &= \left\langle \boldsymbol{D}(\boldsymbol{r}), \frac{\xi(\boldsymbol{r})}{\varepsilon(\boldsymbol{r})}\boldsymbol{D}(\boldsymbol{r})\right\rangle - \langle \xi(\boldsymbol{r})\boldsymbol{D}(\boldsymbol{r}), g(\boldsymbol{r},\boldsymbol{r}'), \xi(\boldsymbol{r}')\boldsymbol{D}(\boldsymbol{r}')\rangle\\ &\quad + \frac{1}{k_0^2}\langle \nabla\cdot[\xi(\boldsymbol{r})\boldsymbol{D}(\boldsymbol{r})], g(\boldsymbol{r},\boldsymbol{r}'), \nabla'\cdot[\xi(\boldsymbol{r}')\boldsymbol{D}(\boldsymbol{r}')]\rangle\\ &\quad - 2\left\langle \boldsymbol{D}(\boldsymbol{r}), \frac{\xi(\boldsymbol{r})}{\varepsilon(\boldsymbol{r})}\boldsymbol{D}^{inc}(\boldsymbol{r})\right\rangle \end{aligned} \tag{8}$$

where

$$\xi(\boldsymbol{r}) = \frac{k^2(\boldsymbol{r}) - k_0^2}{\varepsilon(\boldsymbol{r})} \tag{9}$$

After discretization and through the Rayleigh-Ritz procedure, we can get a similar matrix equation as Eq. (7) by applying $\partial I/\partial D_i = 0$. The equation can be expressed as

$$\begin{aligned}\left\langle \boldsymbol{f}_i(\boldsymbol{r}), \frac{\xi(\boldsymbol{r})}{\varepsilon(\boldsymbol{r})}\boldsymbol{D}^{inc}(\boldsymbol{r})\right\rangle = \sum_j D_j \left\{\left\langle \boldsymbol{f}_i(\boldsymbol{r}), \frac{\xi(\boldsymbol{r})}{\varepsilon(\boldsymbol{r})}\boldsymbol{f}_j(\boldsymbol{r})\right\rangle \right.\\ - \left\langle \xi(\boldsymbol{r})\boldsymbol{f}_i(\boldsymbol{r}), g(\boldsymbol{r},\boldsymbol{r}'), \xi(\boldsymbol{r}')\boldsymbol{f}_j(\boldsymbol{r}')\right\rangle\\ + \frac{1}{k_0^2}\left\langle \nabla\xi(\boldsymbol{r})\cdot\boldsymbol{f}_i(\boldsymbol{r}), g(\boldsymbol{r},\boldsymbol{r}'), \nabla'\xi(\boldsymbol{r}')\cdot\boldsymbol{f}_j(\boldsymbol{r}')\right\rangle\\ + \frac{1}{k_0^2}\left\langle \nabla\xi(\boldsymbol{r})\cdot\boldsymbol{f}_i(\boldsymbol{r}), g(\boldsymbol{r},\boldsymbol{r}'), \xi(\boldsymbol{r}')\nabla'\cdot\boldsymbol{f}_j(\boldsymbol{r}')\right\rangle\\ \left. + \frac{1}{k_0^2}\left\langle \xi(\boldsymbol{r})\nabla\cdot\boldsymbol{f}_i(\boldsymbol{r}), g(\boldsymbol{r},\boldsymbol{r}'), \nabla'\xi(\boldsymbol{r}')\cdot\boldsymbol{f}_j(\boldsymbol{r}')\right\rangle\right. \end{aligned}$$

$$+\frac{1}{k_0^2}\left\langle \xi(\boldsymbol{r})\nabla\cdot\boldsymbol{f}_i(\boldsymbol{r}), g(\boldsymbol{r},\boldsymbol{r}'), \xi(\boldsymbol{r}')\nabla'\cdot\boldsymbol{f}_j(\boldsymbol{r}')\right\rangle\Bigg\}$$
$$=\sum_j Z'_{ij}D_j \tag{10}$$

If the basis functions are divergence free, the above equation can be simplified as

$$\left\langle \boldsymbol{f}_i(\boldsymbol{r}), \frac{\xi(\boldsymbol{r})}{\varepsilon(\boldsymbol{r})}\boldsymbol{D}^{inc}(\boldsymbol{r})\right\rangle = \sum_j D_j\left\{\left\langle \boldsymbol{f}_i(\boldsymbol{r}), \frac{\xi(\boldsymbol{r})}{\varepsilon(\boldsymbol{r})}\boldsymbol{f}_j(\boldsymbol{r})\right\rangle - \left\langle \xi(\boldsymbol{r})\boldsymbol{f}_i(\boldsymbol{r}), g(\boldsymbol{r},\boldsymbol{r}'), \xi(\boldsymbol{r}')\boldsymbol{f}_j(\boldsymbol{r}')\right\rangle + \frac{1}{k_0^2}\left\langle \nabla\xi(\boldsymbol{r})\cdot\boldsymbol{f}_i(\boldsymbol{r}), g(\boldsymbol{r},\boldsymbol{r}'), \nabla'\xi(\boldsymbol{r}')\cdot\boldsymbol{f}_j(\boldsymbol{r}')\right\rangle\right\} \tag{11}$$

3. SWG BASIS AND BASIS REDUCTION SCHEME

The RWG basis for surface mesh [3] and SWG basis for volume mesh [16] are widely used basis. They are suitable for modeling electric currents or electric flux by keeping their normal continuity. The SWG basis function is defined as

$$\boldsymbol{f}_i(\boldsymbol{r}) = \begin{cases} \dfrac{1}{3V^+}\rho^+, & \boldsymbol{r}\in T_n^+, \\ \dfrac{1}{3V^-}\rho^-, & \boldsymbol{r}\in T_n^-, \\ 0, & \text{otherwise.} \end{cases} \tag{12}$$

This definition is slightly different from the one in [3], but it will help to clarify the physics when we consider the basis reduction scheme and the loop basis later.

The divergence of the SWG basis is

$$\nabla\cdot\boldsymbol{f}_i(\boldsymbol{r}) = \begin{cases} \dfrac{1}{V^+}, & \boldsymbol{r}\in T_n^+, \\ -\dfrac{1}{V^-}, & \boldsymbol{r}\in T_n^-, \\ 0, & \text{otherwise.} \end{cases} \tag{13}$$

From the continuity equation

$$\nabla\cdot\boldsymbol{J}(\boldsymbol{r}) = i\omega\rho(\boldsymbol{r}) \tag{14}$$

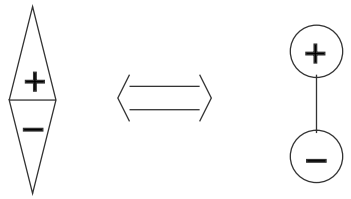

Figure 1. A comparison of the divergence of an RWG basis function with an electric dipole.

we know that the charge density of each basis function is similar to a dipole, as shown in Fig. 1.

Since the divergence of the electric flux is zero everywhere in the scatterer, can we apply the divergence free condition to the matrix equation to improve the accuracy of the computation? One scheme is basis reduction [17]. Its idea is to enforce the divergence free condition in every tetrahedron. It is known that there are 4 SWG basis functions related to one tetrahedron T_i, e.g., $\boldsymbol{f}_1$, $\boldsymbol{f}_2$, $\boldsymbol{f}_3$, $\boldsymbol{f}_4$. The electric flux in T_i can be expressed as

$$\boldsymbol{D}_i(\boldsymbol{r}) = D_1\boldsymbol{f}_1(\boldsymbol{r}) + D_2\boldsymbol{f}_2(\boldsymbol{r}) + D_3\boldsymbol{f}_3(\boldsymbol{r}) + D_4\boldsymbol{f}_4(\boldsymbol{r}) \tag{15}$$

Apply the condition $\nabla \cdot \boldsymbol{D}(\boldsymbol{r}) = 0$,

$$\nabla \cdot \boldsymbol{D}_i(\boldsymbol{r}) = \frac{\pm D_1 \pm D_2 \pm D_3 \pm D_4}{V_i} = 0 \tag{16}$$

i.e.,

$$\pm D_1 \pm D_2 \pm D_3 \pm D_4 = 0 \tag{17}$$

The sign before D_m in the above is determined by direction of the flux in SWG basis, + if the flux is flowing outside T_i, − if the flux is flowing into T_i. With Eq. (17), one of the four unknowns can be expressed as a linear superposition of the other three in the same tetrahedron. Therefore, one unknown is removed. This can be applied to every tetrahedron in the mesh of the scatterer. Assume that there are N_s faces and N_t tetrahedrons, the number of SWG basis functions is the same as the number of faces, i.e., N_s. After basis reduction, the number of unknowns will be reduced to $N_s - N_t$. Hence, a new smaller matrix equation can be generated.

Although it is clear that one SWG basis function in a tetrahedron can be removed, to determine which one to omit is not straightforward because all these tetrahedrons are linked with each other through faces. This can be explained in a simpler two dimensional example. (In two

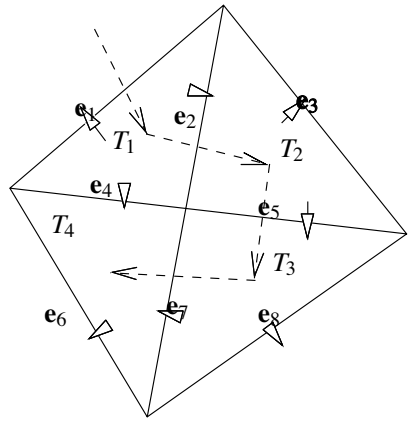

Figure 2. An example of selecting the independent basis in two dimensions.

dimensions, the unknowns are associated with the edges and basis reduction is applied to every triangle.)

Shown in Fig. 2, if we select $\boldsymbol{e}_2$ in T_1 as the reduced basis function, one unknown in T_2 is also reduced. How can we select the reduced basis function in T_2 then? To solve this problem, let us think in the following way: The number of independent basis functions is $N_s - N_t$. If we can delete N_t basis functions from the N_s basis functions without repetition, and at least one basis function is deleted for each tetrahedron, then the basis functions left are independent. To implement this idea, the procedure is to do a depth-first search [18] for all elements (tetrahedrons in volume mesh or triangles in surface mesh). The outside region is also considered as one element where the search procedure starts, each element is visited once and only once. When we move from one element to another, one boundary element (surfaces in tetrahedral mesh or edges in triangular mesh) will be crossed. Since there are N_t tetrahedrons, the total number of faces crossed is also N_t. The basis functions associated with these N_t faces can be regarded as dependent basis and will be eliminated in the new matrix equation.

The surface mesh in Fig. 2 with 4 tetrahedrons and 8 edges illustrates this scheme. A path of depth-first search can be generated as shown in dash lines. The basis functions crossed by this path are $\boldsymbol{e}_1$, $\boldsymbol{e}_2$, $\boldsymbol{e}_5$, $\boldsymbol{e}_7$. Therefore, the independent basis functions are $\boldsymbol{e}_3$, $\boldsymbol{e}_4$, $\boldsymbol{e}_6$, $\boldsymbol{e}_8$. The divergence-free condition can be written into a

matrix form [19]

$$\overline{\boldsymbol{T}}_0 \cdot \boldsymbol{J} = \begin{pmatrix} 1 & 1 & 0 & 1 & 0 & 0 & 0 & 0 \\ 0 & -1 & 1 & 0 & 1 & 0 & 0 & 0 \\ 0 & 0 & 0 & 0 & -1 & 0 & 1 & 1 \\ 0 & 0 & 0 & -1 & 0 & 1 & -1 & 0 \end{pmatrix} \cdot \begin{pmatrix} j_1 \\ j_2 \\ j_3 \\ j_4 \\ j_5 \\ j_6 \\ j_7 \\ j_8 \end{pmatrix} = \mathbf{0} \tag{18}$$

or

$$\begin{pmatrix} j_3 \\ j_4 \\ j_6 \\ j_8 \\ j_1 \\ j_2 \\ j_5 \\ j_7 \end{pmatrix} = \begin{pmatrix} 1 & 0 & 0 & 0 \\ 0 & 1 & 0 & 0 \\ 0 & 0 & 1 & 0 \\ 0 & 0 & 0 & 1 \\ -1 & 0 & -1 & -1 \\ 1 & -1 & 1 & 1 \\ 0 & -1 & 1 & 1 \\ 0 & -1 & 1 & 0 \end{pmatrix} \cdot \begin{pmatrix} j_3 \\ j_4 \\ j_6 \\ j_8 \end{pmatrix} = \overline{\boldsymbol{T}} \cdot \boldsymbol{J}_{indp} \tag{19}$$

where $\boldsymbol{J}_{indp}$ is the left-over basis set and $\overline{\boldsymbol{T}}$ is the transformation matrix. Hence, a new matrix equation can be derived as

$$\overline{\boldsymbol{Z}}' \cdot \boldsymbol{J}_{indp} = \overline{\boldsymbol{T}}^{\dagger} \cdot \overline{\boldsymbol{Z}} \cdot \overline{\boldsymbol{T}} \cdot \boldsymbol{J}_{indp} = \overline{\boldsymbol{T}}^{\dagger} \cdot \boldsymbol{V} \tag{20}$$

The original matrix element Z_{ij} in the matrix equation is

$$Z_{ij} = \left\langle \boldsymbol{f}_i(\boldsymbol{r}), \overline{\boldsymbol{L}}(\boldsymbol{r}, \boldsymbol{r}'), \boldsymbol{f}_j(\boldsymbol{r}) \right\rangle \tag{21}$$

After basis reduction, the new matrix element Z'_{ij} in Eq. (20) is

$$Z'_{ij} = \left\langle \sum_{k=0}^{N} T_{ki} \boldsymbol{f}_k, \overline{\boldsymbol{L}}(\boldsymbol{r}, \boldsymbol{r}'), \sum_{k=0}^{N} T_{kj} \boldsymbol{f}_k \right\rangle \tag{22}$$

It can be seen that $\sum_{k=0}^{N} T_{ki} \boldsymbol{f}_k$ generates the new basis functions. They turn out to be loop basis functions. As in Fig. 2, the new basis functions are

$$\begin{aligned} \boldsymbol{I}_1 &= -\boldsymbol{e}_1 + \boldsymbol{e}_2 + \boldsymbol{e}_3 \\ \boldsymbol{I}_2 &= -\boldsymbol{e}_2 + \boldsymbol{e}_4 - \boldsymbol{e}_5 - \boldsymbol{e}_7 \\ \boldsymbol{I}_3 &= -\boldsymbol{e}_1 + \boldsymbol{e}_2 + \boldsymbol{e}_5 + \boldsymbol{e}_6 + \boldsymbol{e}_7 \\ \boldsymbol{I}_4 &= -\boldsymbol{e}_1 + \boldsymbol{e}_2 + \boldsymbol{e}_5 + \boldsymbol{e}_8 \end{aligned} \tag{23}$$

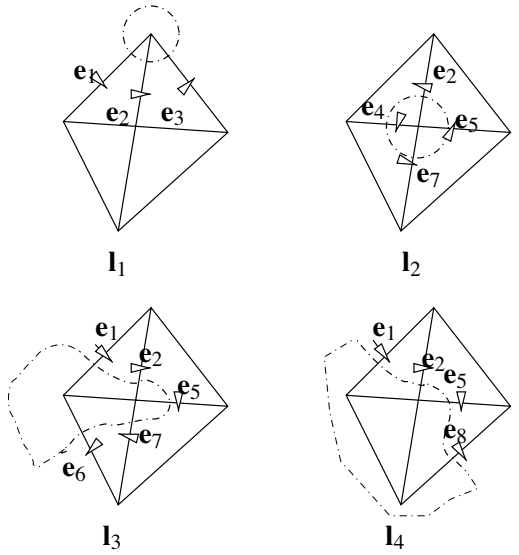

Figure 3. The independent basis functions after basis reduction.

It can be seen from Fig. 3 that each new basis function forms a closed loop if only we take the outside region as one element. Moreover, the loop basis set shown in Fig. 3 is not unique. If we select another search path, a different loop basis set will be generated. This basis reduction scheme can be applied directly to a volume mesh if only we change triangles and edges to tetrahedrons and faces.

The advantage of the basis reduction scheme is a decrease in the number of unknowns. However, because the overlaps increase among the new basis functions, the matrix equation will have a larger condition number. Therefore, solving the matrix equation with iterative methods is difficult. A comparison in the number of unknowns using full SWG basis and SWG basis after reduction in the number of unknowns and the iteration count using the CGNR method is shown in Tab. 1.

4. LOOP BASIS FROM VOLUME MESH

The second way of applying the divergence-free condition is to use the loop basis, which is inherently solenoidal. The volume loop basis in three dimensions is defined as [12]

$$\boldsymbol{O}_i(\boldsymbol{r}) = \sum_{k=1}^{N_k} \frac{\boldsymbol{L}_k}{V_k} f_k(\boldsymbol{r}) \tag{24}$$

Table 1. A comparison of the iteration count of using the CGNR method to solve the matrix equation of SWG basis and basis after reduction. The example used here is a plane wave scattering problem by a dielectric sphere.

Tet No	SWG No	Dens	It No (1e-3)	Red Basis	Red Ratio(%)	It No
506	783	8.57	100	626	44.70	$> 400(2.19\text{E}-2)$
571	1276	10.09	106	705	44.70	$> 400(3.47\text{E}-2)$
605	1344	10.26	106	739	45.01	$> 400(3.73\text{E}-2)$
786	1681	11.06	108	897	46.60	$> 400(3.47\text{E}-2)$
1123	2465	12.56	120	1342	45.60	$> 400(6.40\text{E}-2)$

where N_k is the total number of tetrahedrons attached to the ith edge and

$$f_k(\boldsymbol{r}) = \begin{cases} 1, & \boldsymbol{r} \in T_k, \\ 0, & \boldsymbol{r} \in \text{elsewhere}. \end{cases} \tag{25}$$

The vector $\boldsymbol{L}_k$ is parallel with the edge that is opposite to the common edge in the kth tetrahedron. An example of a loop basis function in three dimensions is shown in Fig. 4.

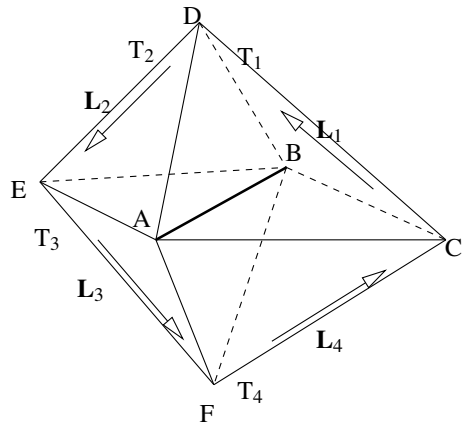

Figure 4. An example of volume loop basis in three dimensions.

At the boundary, a half loop basis can be defined associated with the boundary edges. It can also be considered as a full loop basis with virtual outside tetrahedrons of relative permittivity $\varepsilon_r = 1$. One example of half volume loop basis is shown in Fig. 5.

Similar as in the two-dimensional case, a loop basis function can

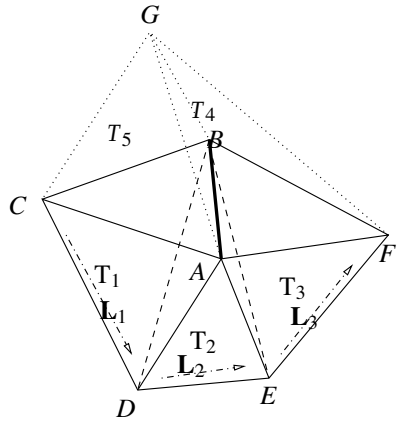

Figure 5. An example of half volume loop basis.

be considered as a linear superposition of several SWG basis functions, and the divergence of a loop basis function is zero. Even so, the loop basis also keeps the continuity of normal flux. It can be proved that the number of independent loop basis functions N_{loop} is

$$N_{loop} = N_s - N_t = N_e - N_v + 1 \tag{26}$$

where N_s is the number of faces, N_t is the number of tetrahedrons, N_v is the number of vertices, and N_e is the number of edges. The basis set in this statement includes both the full basis and half basis functions. It also tells us that if only we can find N_{loop} independent loop basis functions, they constitute a complete set. In the case of one tetrahedron, there are six edges. However, only three are needed to describe the divergence-free flux in this tetrahedron as shown in Fig. 6.

A question to answer before applying the volume loop basis is on setting up the independent loop basis set from the geometrical mesh instead of the complex matrix manipulation. There are at least two ways available to set up the minimum and complete basis set: basis reduction and generating tree. The basis reduction scheme is based on the fact that the new basis set after basis reduction is actually a set of loop basis. However, there are many overlaps between these loops that generate a poorly-conditioned matrix. Although some orthogonalization scheme can be used to reduce the correlation among basis functions, the numerical complexity will increase as in [12] and [14].

The generating tree scheme is based on the connecting information in a geometrical mesh. It has been applied in searching for loop basis

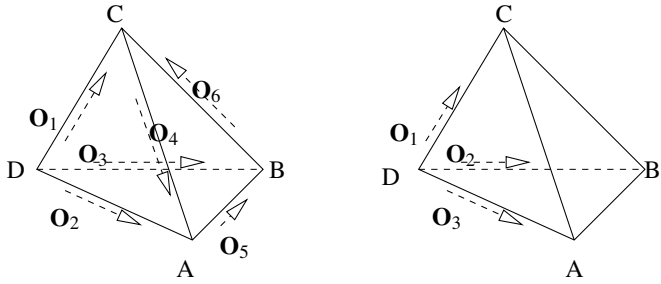

Figure 6. Example of finding independent loop basis in one tetrahedron.

functions from surface mesh [20, 19]. In this scheme, the geometrical mesh can be considered as an undirected graph (undigraph) [18] with tetrahedrons as nodes and faces as edges. The outer space needs to be considered as one polyhedron, i.e., another node in the undigraph. A generating tree of this undigraph connects all the tetrahedrons with a minimal number of faces. The number of left-over faces is equal to the number of loop basis functions according to Eq. (26). Therefore, when every left-over face is put into the generating tree to construct a new undigraph, one loop basis function can be found from it. Similar to surface loop basis, the loop basis function generated using this scheme may not be minimal, the algorithm of reducing the loop to a minimum can be found in [20].

To reduce the complexity of minimizing the loop basis functions, another generating tree scheme can be used in volume mesh. Instead of constructing the graph of tetrahedrons and faces, nodes and edges in a geometrical mesh can also be used to set up an undigraph. The generating tree of this new undigraph links the N_v nodes with $N_v - 1$ edges. The number of left-over edges are just $N_e - N_v + 1$. According to Eq. (26), this number is equal to the number of volume loop basis functions. Therefore, these left-over edges can form an independent volume loop basis set. The advantage of this scheme is that every loop basis function defined from this scheme is a minimal one; we do not need the additional step of minimizing each loop basis function. The limitation of this method is that it is only valid for simply connected region, i.e., an object without holes. If the object is not simply connected, the second identity in Eq. (26) is not true.

Fig. 7 shows one example of generating loop basis functions from a diamond shape geometry. The thin dot-dashed lines with arrows indicate a tree constructed by tetrahedrons and faces $T_1 \rightarrow T_2 \rightarrow T_4 \rightarrow T_3$. The solid dots indicate the independent loop basis defined

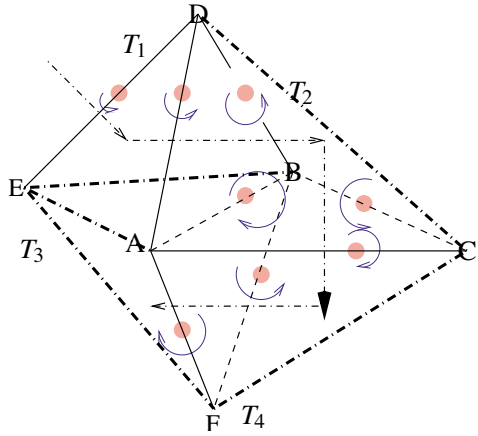

Figure 7. An example of generating volume loop basis from the tree in an undigraph.

associated with the corresponding edges. The thick dashed lines indicate another generating tree linking nodes together through edges. It shows that the two trees can generate the same set of loop basis.

Moreover, Eq. (26) shows that the number of independent volume loop basis functions is the same with the number of basis functions after basis reduction. The loop basis can also be regarded as a rearrangement of the SWG basis. Similar to the basis reduction scheme, the matrix equation constructed using independent loop basis is poorly conditioned. Although the number of unknowns decreases more than 1/3, the iteration count increases. Therefore, these two methods are suitable for direct matrix solvers, such as LU decomposition.

5. VOLUME LOOP BASIS ON EVERY EDGE

Although loop basis functions keep the divergence free condition and the normal continuity of flux, the poorly-conditioned matrix they generate is detrimental to iterative matrix solvers. Hence a remedy needs to be found.

One solution to improving the convergence of iterative solvers is to expand this set to every possible candidate of loop basis functions. Obviously, the basis functions in this new set are not independent of each other any more. A null space exists in this matrix equation. However, this null space will not worsen the condition of the matrix

solver but speed up the convergence of solutions when an iterative solver is used. Although it seems that introducing a null space to the matrix is harmful, it turns out that this null space is not detrimental if only the right hand side vector is used as an initial guess. A proof is given in the Appendix.

Beside a mathematical proof, the reason can also be analyzed heuristically: Expanded loop basis set gives more freedom for the solution of flux to converge to the correct result than the minimal basis set, hence iterative solvers converge faster.

Beside the improvement on convergence, there are several advantages in using the expanded loop basis set. Because the loop basis functions are defined associated with every edge, the selection of a basis set is much simpler; there is no need to execute the particular algorithm to determine which loop to keep and which to abandon. Moreover, the scheme to construct this expanded basis set is not restricted to simply connected objects, which makes it more general.

6. NUMERICAL EXAMPLES

Some numerical examples will be shown here to validate the algorithm of volume loop basis functions.

6.1. A Plane Wave Scattered by a Dielectric Sphere

In this example, a 0.1 GHz plane wave is scattered by a dielectric sphere with radius 1 m and relative permittivity $\varepsilon_r = 4.0$. The incident angle is $\theta = 180^\circ$, $\phi = 0^\circ$. The sphere is discretized into 3,928 tetrahedrons with 8,437 SWG basis functions defined with the unknown density 19.8 per wavelength in the dielectric medium. Consequently, 5,487 loop basis functions are defined associated with every edge. The unknown density is 16.4 per wavelength in the dielectric medium. The number of unknowns using loop basis is reduced by 34.97%. The CG method is used to solve these two matrix equations. It takes 119 iterations (2 min 55 sec) to solve the matrix equation of SWG basis and 152 iterations (1 min 33 sec) to solve the matrix equation of loop basis. Although the iteration count is larger for the loop basis, the solving time is still shorter because of fewer unknowns. The results of radar cross section (RCS) using SWG basis and volume loop basis functions are plotted in Fig. 8. The two curves overlap with each other and are very closed to the Mie series solution. Therefore, using loop basis, this problem can be solved with fewer unknowns to the same accuracy as the SWG basis.

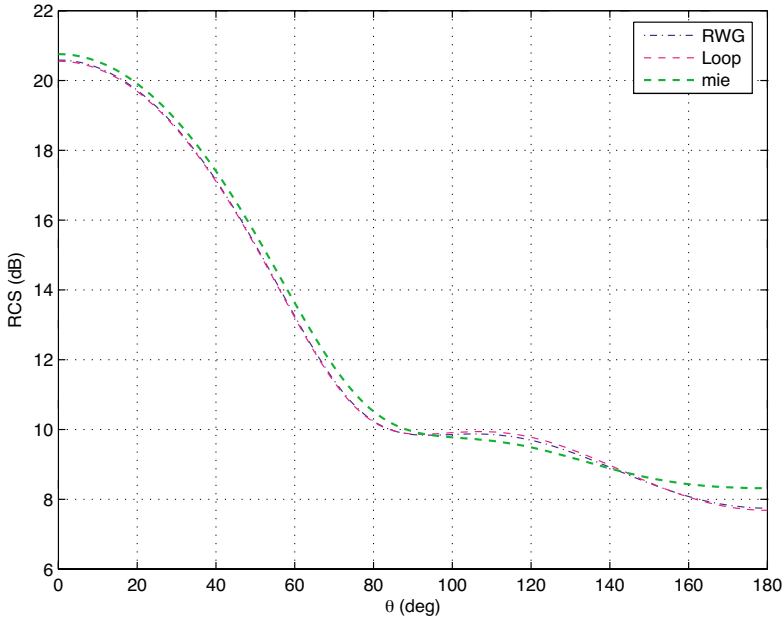

Figure 8. RCS of a 0.1 GHz plane wave scattered by a dielectric sphere with $\varepsilon_r = 4.0$. The radius of the sphere is 1 meter.

6.2. A Plane Wave Scattered by a Dielectric Ring

As shown in Fig. 9, the model in this simulation is a dielectric ring. The dimension of this ring is shown in the figure, ε_r is set to be 4 in this example. This object is discretized into 3,331 tetrahedrons with 7,356 SWG basis functions (11.5 per wavelength in the medium) defined associated with every surface and 4,965 (10.05 per wavelength in the medium) loop basis functions are defined associated with every edge. The number of basis functions is reduced by 32.5%. The incident 1 GHz plane wave comes from $-\hat{\boldsymbol{z}}$ to $+\hat{\boldsymbol{z}}$ direction. The CGNR method is used in the matrix solver.

It takes 159 iterations for the matrix equation of SWG basis to converge to 10^{-3} and 390 iterations for the equation of loop basis to converge to the same error criteria. In the results of RCS plotted in Fig. 10, the three curves are very close to each other. The solid line indicates the RCS computed using SWG basis with a denser mesh to represent the accurate solution. From this example, it validates our treatment for the object with holes when using expanded volume loop basis set associated every edge. Therefore, unlike surface loop basis functions, volume basis functions could be defined on every edge

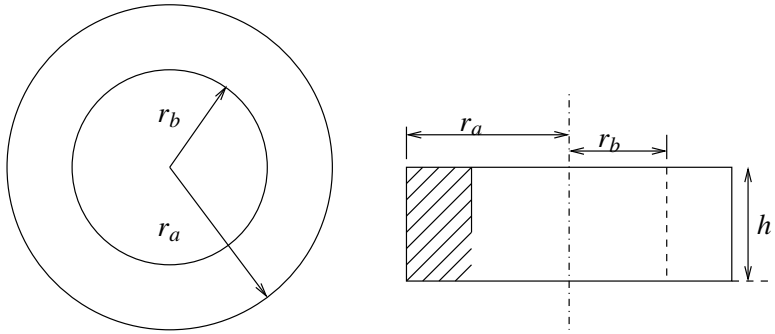

Figure 9. The dielectric ring model with $r_a = 0.25\,\text{m}$, $r_b = 0.1\,\text{m}$, $h = 0.1\,\text{m}$.

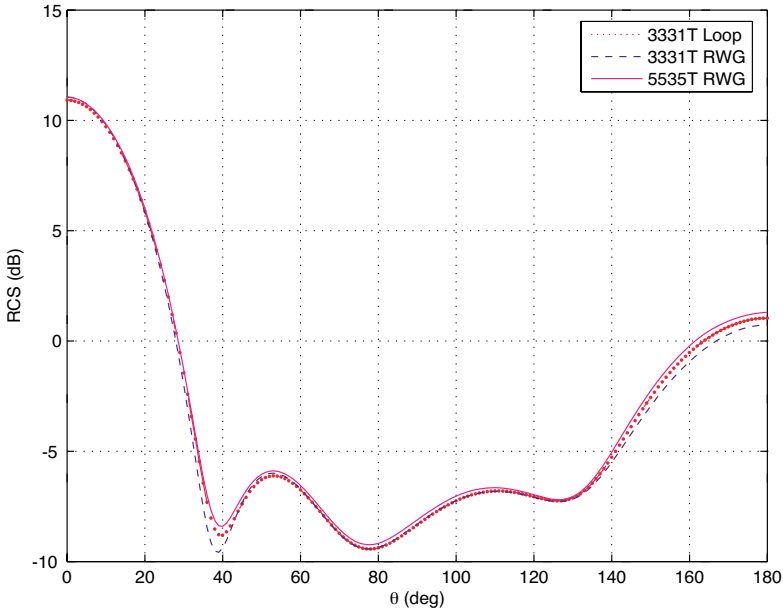

Figure 10. RCS of the dielectric ring with plane wave incident at 1 GHz.

directly without executing the complicated search algorithms.

These two examples imply that we could get correct results with the same accuracy using expanded volume loop basis functions. The number of unknowns in these two examples is also greatly reduced compared with the tetrahedral SWG basis (around 30–40%).

Moreover, the construction of the basis functions is straightforward and faster than that of the surface loop basis.

7. CONCLUSION

In this paper, the application of the divergence free condition in solving the VIE is discussed. Several schemes can be used, such as the basis reduction scheme, the minimal complete volume loop basis set. Both of them will generate a poorly-conditioned matrix. A better way is to use the volume loop basis functions with respect to every edge. In spite of the existence of a null space in the matrix, an iterative solver can still be used to stably solve the matrix equation. Using this scheme, the number of unknowns can be reduced by 30–40% compared with the number of SWG basis. Moreover, the complicated algorithm of constructing loop basis is not necessary.

APPENDIX A. PROOF OF CONVERGENCE OF ITERATIVE SOLVERS USING EXPANDED VOLUME LOOP BASIS SET

In this section, we will prove that the matrix equation of the expanded volume loop basis set can still be solved by iterative solver even with the existence of a null space in the matrix.

Suppose the matrix equation using the expanded loop basis set is

$$\overline{\boldsymbol{Z}}_{l0} \cdot \boldsymbol{J}_{l0} = \boldsymbol{V}_{l0} \tag{A1}$$

$\boldsymbol{J}_{l0}$ contains two part: the independent basis set $\boldsymbol{J}_{ln}$ and the dependent basis set $\boldsymbol{J}_{ld}$ that can be expressed as a linear superposition of elements in the independent basis set. Rearrange the indices of the basis functions so that the two parts are separate in the matrix, i.e.

$$\boldsymbol{J}_{l0} = \left[\boldsymbol{J}_{ln}^T \quad \boldsymbol{J}_{ld}^T\right]^T \tag{A2}$$

The matrix $\overline{\boldsymbol{Z}}_{l0}$ is then partitioned into four parts,

$$\begin{bmatrix} \overline{\boldsymbol{Z}}_{nn} & \overline{\boldsymbol{Z}}_{nd} \\ \overline{\boldsymbol{Z}}_{dn} & \overline{\boldsymbol{Z}}_{dd} \end{bmatrix} \cdot \begin{bmatrix} \boldsymbol{J}_{ln} \\ \boldsymbol{J}_{ld} \end{bmatrix} = \begin{bmatrix} \boldsymbol{V}_{ln} \\ \boldsymbol{V}_{ld} \end{bmatrix} \tag{A3}$$

$\overline{\boldsymbol{Z}}_{l0}$ contains a null space due to the dependent basis set. Its rank is equal to the rank of $\overline{\boldsymbol{Z}}_{nn}$.

The following corollaries will help us to prove that $\overline{\boldsymbol{Z}}_{l0}$ can still be solved iteratively.

Corollary 1 *If* $\overline{\boldsymbol{A}}$ *is a diagonalizable matrix, span* $\{\boldsymbol{v} : \boldsymbol{v} = \overline{\boldsymbol{A}} \cdot \boldsymbol{x} \in \mathcal{R}^n\}$ *is always orthogonal to null* $(\overline{\boldsymbol{A}})$.

Proof: $\overline{\boldsymbol{A}}$ can be diagonalizable as $\overline{\boldsymbol{A}} = \overline{\boldsymbol{U}} \cdot \overline{\Lambda} \cdot \overline{\boldsymbol{U}}^{-1}$. Where $\overline{\Lambda} = diag\{\lambda_1, \lambda_2, \ldots, \lambda_n\}$, $\overline{\boldsymbol{U}} = [\boldsymbol{u}_1, \boldsymbol{u}_2, \boldsymbol{u}_3, \ldots, \boldsymbol{u}_n]$. $\boldsymbol{u}_i$ is the eigenvector with eigenvalue λ_i. A vector $\boldsymbol{x}$ can be expressed as a linear superposition of $\boldsymbol{u}_i$, i.e., $\boldsymbol{x} = \sum_{i=0}^{n} a_i \boldsymbol{u}_i$. Therefore, $\overline{\boldsymbol{A}} \cdot \boldsymbol{x} = \sum_{i=0}^{n} a_i \overline{\boldsymbol{A}} \cdot \boldsymbol{u}_i = \sum_{i=0}^{n} a_i \lambda_i \boldsymbol{u}_i = \sum_{i=0, \lambda_i \neq 0}^{n} a_i \lambda_i \boldsymbol{u}_i$. The eigenvector with eigenvalue 0 will have no contribution to $\overline{\boldsymbol{A}} \cdot \boldsymbol{x}$. So $\overline{\boldsymbol{A}} \cdot \boldsymbol{x}$ is only in the space orthogonal to *null* $(\overline{\boldsymbol{A}})$. □

Corollary 2 *The right-hand side (RHS) vector in the matrix equation of expanded loop basis set,* $\boldsymbol{V}_{l0}$*, lies in the range of the impedance matrix* $\overline{\boldsymbol{A}}_{l0}$*, i.e.,* $\boldsymbol{V}_{l0} \in ran\ (\overline{\boldsymbol{A}}_{l0})$.

Proof: As it is known, an independent loop basis set can be found from the expanded loop basis set (defined on every edge). The matrix equation of this minimal loop basis set is

$$\overline{\boldsymbol{Z}}_{nn} \cdot \boldsymbol{J}_{ln} = \boldsymbol{V}_{ln} \tag{A4}$$

The matrix equation of the expanded loop basis is expressed as

$$\overline{\boldsymbol{Z}}_{l0} \cdot \boldsymbol{J}_{l0} = \boldsymbol{V}_{l0} \tag{A5}$$

By rearranging the basis functions, we can get

$$\overline{\boldsymbol{Z}}_{l0} = \begin{bmatrix} \overline{\boldsymbol{Z}}_{nn} & \overline{\boldsymbol{Z}}_{nd} \\ \overline{\boldsymbol{Z}}_{dn} & \overline{\boldsymbol{Z}}_{dd} \end{bmatrix} = \overline{\boldsymbol{T}} \cdot \overline{\boldsymbol{Z}}_{nn} \cdot \cdot \overline{\boldsymbol{T}}^{t} \tag{A6}$$

where $\overline{\boldsymbol{T}} \in \mathcal{R}^{m \times n}$, and $m > n$. This is because every basis function used in $\overline{\boldsymbol{Z}}_{l0}$ can be expressed as a linear superposition of basis functions used in $\overline{\boldsymbol{Z}}_{nn}$. Similarly, the RHS vector of full loop basis $\boldsymbol{V}_{l0}$ can also be set up from the RHS of minimal loop basis by

$$\boldsymbol{V}_{l0} = \overline{\boldsymbol{T}} \cdot \boldsymbol{V}_{ln} \tag{A7}$$

The solution of the current $\boldsymbol{J}_{l0}$ satisfies

$$\boldsymbol{J}_{l0} = \overline{\boldsymbol{T}}^{t'} \cdot \boldsymbol{J}_{ln} \tag{A8}$$

where $\overline{\boldsymbol{T}}^{t'}$ is the pseudo inverse of $\overline{\boldsymbol{T}}^{t}$. The existence of $\overline{\boldsymbol{T}}^{t'}$ is validated [21]. Because $m > n$, $\overline{\boldsymbol{T}}^{t} \cdot \overline{\boldsymbol{T}}^{t'} = \overline{\boldsymbol{I}}_{n \times n}$.

Since the the basis functions used in $\overline{\boldsymbol{Z}}_{nn}$ are independent of each other, $\overline{\boldsymbol{Z}}_{nn}$ is a full matrix, there exists a solution $\boldsymbol{J}_{ln}$ to Eq. (A4).

Therefore, we can insert an identity matrix between $\overline{\boldsymbol{Z}}_{nn}$ and $\overline{\boldsymbol{J}}_{ln}$.

$$\overline{\boldsymbol{Z}}_{nn} \cdot \overline{\boldsymbol{T}}^{t} \cdot \overline{\boldsymbol{T}}^{t'} \cdot \boldsymbol{J}_{ln} = \boldsymbol{V}_{ln} \tag{A9}$$

Multiply $\overline{\boldsymbol{T}}$ on both sides,

$$\overline{\boldsymbol{T}} \cdot \overline{\boldsymbol{Z}}_{nn} \cdot \overline{\boldsymbol{T}}^{t} \cdot \overline{\boldsymbol{T}}^{t'} \cdot \boldsymbol{J}_{ln} = \overline{\boldsymbol{T}} \cdot \boldsymbol{V}_{ln} \tag{A10}$$

i.e.,

$$\overline{\boldsymbol{Z}}_{l0} \cdot \boldsymbol{J}_{l0} = \boldsymbol{V}_{l0} \tag{A11}$$

Hence, there exists $\boldsymbol{J}_{l0} = \overline{\boldsymbol{T}}^{t'} \cdot \boldsymbol{J}_{l0}$ satisfies Eq. (A5). This tells us $\boldsymbol{V}_{l0} \in ran\ (\overline{\boldsymbol{Z}}_{l0})$. □

Theorem 1 *The matrix equation of the expanded loop basis, i.e., Eq. (A3), can still be solved using conjugate gradient (CG) method even a null space exists in* $\overline{\boldsymbol{Z}}_{l0}$.

Proof: When CG method is used, we assign the initial guess of the solution as the RHS vector. It is known that the solution of the matrix equation using CG method as the solver will always be in the space spanned by $\left\{\boldsymbol{r}_0, \overline{\boldsymbol{Z}}_{l0} \cdot \boldsymbol{r}_0, \overline{\boldsymbol{Z}}_{l0}^2 \cdot \boldsymbol{r}_0, \ldots, \overline{\boldsymbol{Z}}_{l0}^n \cdot \boldsymbol{r}_0\right\}$, i.e., the Krylov space [22]. Because the initial guess $\boldsymbol{r}_0 = \boldsymbol{V}_{l0} \in ran\ (\overline{\boldsymbol{Z}}_{l0})$, according to Theorem 1, this Krylov space is in the range of $\overline{\boldsymbol{Z}}_{l0}$. So the solution vector will never fall into *null* $(\overline{\boldsymbol{A}})$. Since the convergence of the solution is determined by its projection onto the Krylov space, it has nothing to do with the zero eigenvalues. It has been proved that the right hand side vector $\boldsymbol{V}_{l0}$ is in the range of $\overline{\boldsymbol{Z}}_{l0}$, i.e., in the Krylov space. Both the solution and the right hand side vector are not related with the null space of $\overline{\boldsymbol{Z}}_{l0}$. We can conclude that the solution vector can converge correctly. □

Fig. A1 shows one example of the eigenvalue distribution of $\overline{\boldsymbol{Z}}_{l0}$ and $\overline{\boldsymbol{Z}}_{ln}$. It can be seen that $\overline{\boldsymbol{Z}}_{ln}$ has no zero eigenvalues, i.e., this matrix does not contain null space. $\overline{\boldsymbol{Z}}_{l0}$ has several zero eigenvalues which make the matrix ill-conditioned. However, the ratio of the largest eigenvalue to the smallest non-zero eigenvalue is much smaller than the ratio of $\overline{\boldsymbol{Z}}_{ln}$. This is the mathematical reason of the faster convergence of $\overline{\boldsymbol{Z}}_{l0}$ than $\overline{\boldsymbol{Z}}_{ln}$.

In the above proof, the assumption is that all the vectors are exact without numerical error. But numerical error is inevitable during the computation. This numerical error will bring into the solution vector some components in $null(\overline{\boldsymbol{Z}}_{l0})$. If CG method is not stable with this error, an accurate solution cannot be achieved. The next theorem proves that this numerical error will not affect this convergence of CG

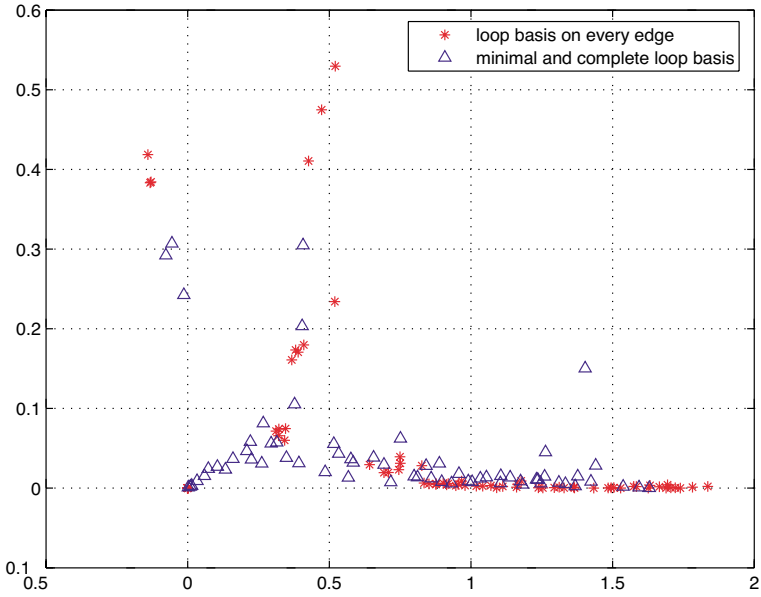

Figure A1. An example of the eigenvalue distribution of $\overline{\boldsymbol{Z}}_{l0}$ and $\overline{\boldsymbol{Z}}_{ln}$.

method, i.e., the result will converge to the solution within machine precision.

Theorem 2 *In the matrix equation* $\overline{\boldsymbol{A}} \cdot \boldsymbol{x} = \boldsymbol{b}$*, the convergence of CG method is stable.*

Proof: The convergence of CG method is determined by the residue $\boldsymbol{r}_n$. The iterative process will end when

$$\frac{\|\boldsymbol{r}_n\|}{\|\boldsymbol{b}\|} = \frac{\|\boldsymbol{b} \cdot \overline{\boldsymbol{A}} \cdot \boldsymbol{x}_n\|}{\|\boldsymbol{b}\|} \leq Err \tag{A12}$$

$\|\boldsymbol{x}\|$ indicates the L_2 norm of $\boldsymbol{x}$. In the practical algorithm, $\boldsymbol{r}_n$ is computed from $\boldsymbol{r}_{n-1}$ instead of from definition. $\boldsymbol{x}_n$ is related with $\boldsymbol{r}_n$ through intermediate vectors $\boldsymbol{p}_n$ and $\boldsymbol{w}_n$. They satisfy the following relations [22]

$$\boldsymbol{p}_1 = \boldsymbol{r}_0 \tag{A13}$$
$$\boldsymbol{p}_k = \boldsymbol{r}_{k-1} + \beta_{k-1}\boldsymbol{p}_{k-1} \tag{A14}$$
$$\boldsymbol{w}_k = \overline{\boldsymbol{A}} \cdot \boldsymbol{p}_k \tag{A15}$$
$$\boldsymbol{x}_k = \boldsymbol{x}_{k-1} + \alpha_k \boldsymbol{p}_k \tag{A16}$$

$$\boldsymbol{r}_k = \boldsymbol{r}_{k-1} - \alpha_k \boldsymbol{w}_k \tag{A17}$$

$$\rho_{k-1} = \boldsymbol{r}_{k-1}^T \boldsymbol{r}_{k-1} \tag{A18}$$

$$\beta_{k-1} = \rho_{k-1}/\rho_{k-2} \tag{A19}$$

$$\alpha_k = \rho_{k-1}/\left(\boldsymbol{p}_k^T \cdot \boldsymbol{q}_k\right) \tag{A20}$$

The numerical error of $\boldsymbol{x}$ comes from the operation of Eq. (A16), and the error of $\boldsymbol{r}$ comes from Eq. (A17). Assume $\boldsymbol{p}_k$ is not purely orthogonal to *null* $(\overline{\boldsymbol{A}})$, i.e., $\boldsymbol{p}_k = \boldsymbol{p}_{k0} + \varepsilon \boldsymbol{p}_{k1}$, where $\boldsymbol{p}_{k0} \in$ *ran* $(\overline{\boldsymbol{A}})$, $\boldsymbol{p}_{k1} \in$ *null* $(\overline{\boldsymbol{A}})$.

As it is known from Eq. (A17), $\boldsymbol{r}_k = \boldsymbol{r}_{k-1} - \alpha_k \overline{\boldsymbol{A}} \cdot (\boldsymbol{p}_{k0} + \varepsilon \boldsymbol{p}_{k1}) = \boldsymbol{r}_{k-1} - \alpha_k \overline{\boldsymbol{A}} \cdot \boldsymbol{p}_{k0}$. Because $\boldsymbol{r}_0 = \boldsymbol{b} \in ran\ (\overline{\boldsymbol{A}})$, $\boldsymbol{r}_k$ is not sensitive to $\boldsymbol{p}_{k1}$, i.e., the convergence of CG method will not be affected.

Similarly, it can be derived from Eq. (A14) that $\boldsymbol{p}_k = \boldsymbol{r}_{k-1} + \beta_k \boldsymbol{p}_{(k-1)0} + \beta_{k-1} \varepsilon \boldsymbol{p}_{(k-1)1}$. Because $\boldsymbol{r}_k$ is immune from the error term $\varepsilon \boldsymbol{p}_{k1}$ and $\beta_{k-1} = \|\boldsymbol{r}_{k-1}\|/\|\boldsymbol{r}_{k-2}\| < 1$ during the iteration if only $\boldsymbol{r}_k$ converges, the error from $\varepsilon_{k-1} \boldsymbol{p}_{(k-1)1}$ will be decreased.

The iterative solution $\boldsymbol{x}_k = \boldsymbol{x}_{k-1} + \alpha_k (\boldsymbol{p}_{k0} + \varepsilon \boldsymbol{p}_{k1})$ will contain some numerical error which causes $\boldsymbol{x}_k \notin ran\ (\overline{\boldsymbol{A}})$. But the error will be limited because the error of $\boldsymbol{p}_k$ is limited.

Therefore, the numerical error will not affect the convergence of CG method and the error of the solution vector is also limited. □

REFERENCES

1. Born, M. and E. Wolf, *Principles of Optics: Electromagnetic Theory of Propagation, Interference and Diffraction of Light*, 7th ed., Cambridge University Press, Cambridge [England]; New York, 1999.
2. Chew, W. C., *Waves and Fields in Inhomogeneous Media*, IEEE Press, New York, 1995.
3. Schaubert, D., D. Wilton, and A. Glisson, "A tetrahedral modeling method for electromagnetic scattering by arbitrarily shaped inhomogeneous dielectric bodies," *IEEE Trans. Antennas Propagat.*, Vol. 32, No. 1, 77–85, Jan. 1984.
4. Richmond, J., "Scattering by a dielectric cylinder of arbitrary cross section shape," *IEEE Trans. Antennas Propagat.*, Vol. 13, No. 3, 334–341, May 1965.
5. —, "TE-wave scattering by a dielectric cylinder of arbitrary cross-section shape," *IEEE Trans. Antennas Propagat.*, Vol. 14, No. 4, 460–464, July 1966.

6. Rubin, B. J., "Divergence-free basis for representing polarization current in finite-size dielectric regions," *IEEE Trans. Antennas Propagat.*, Vol. 41, No. 3, 269–277, Mar. 1993.
7. Wu, W. L., A. Glisson, and D. Kajfez, "A study of two numerical solution procedures for the electric field integral equation at low frequency," *ACES J.*, Vol. 10, No. 3, 69–80, Nov. 1995.
8. Vecchi, G., "Loop-star decomposition of basis functions in the discretization of the EFIE," *IEEE Trans. Antennas Propagat.*, Vol. 47, No. 2, 339–346, Feb. 1999.
9. Zhao, J. S. and W. C. Chew, "Integral equation solution of Maxwell's equations from zero frequency to microwave frequencies," *IEEE Trans. Antennas Propagat.*, Vol. 48, No. 10, 1635–1645, Oct. 2000.
10. Lee, J. F., R. Lee, and R. J. Burkholder, "Loop star basis functions and a robust pre-conditioner for EFIE scattering problems," *IEEE Trans. Antennas Propagat.*, Vol. 51, No. 8, 1855–1863, Aug. 2003.
11. Eibert, T. F., "Iterative-solver convergence for loop-star and loop-tree decompositions in method-of-moments solutions of the electric-field integral equation," *IEEE Antennas Propagat. Mag.*, Vol. 46, No. 3, 80–85, June 2004.
12. Mendes, L. S. and S. A. Carvalho, "Scattering of EM waves by homogeneous dielectrics with the use of the method of moments and 3D solenoidal basis functions," *Micro. Opt. Tech. Lett.*, Vol. 12, No. 6, 327–331, Aug. 1996.
13. Carvalho, S. A. and L. S. Mendes, "Scattering of EM waves by inhomogeneous dielectrics with the use of the method of moments and the 3D solenoidal basis functions," *Micro. Opt. Tech. Lett.*, Vol. 23, No. 1, 42–46, Oct. 1999.
14. Kulkarni, S., R. Lemdiasov, R. Ludwig, and S. Makarov, "Comparison of two sets of low-order basis functions for tetrahedral VIE modeling," *IEEE Trans. Antennas Propagat.*, Vol. 52, No. 10, 2789–2794, Oct. 2004.
15. Gan, H. and W. C. Chew, "A discrete BCG-FFT algorithm for solving 3D inhomogeneous scatterer problems," *J. Electromagn. Waves Appl.*, Vol. 9, No. 10, 1339–1357, 1995.
16. Rao, G. R. W. S. M and A. W. Glisson, "Electromagnetic scattering by surfaces of arbitrary shape," *IEEE Trans. Antennas Propagat.*, Vol. 30, No. 3, 409–418, May 1982.
17. Chao, H.-Y. R., "A multilevel fast multipole algorithm for analyzing radiation and scattering from wire antennas in a complex environment," Ph.D. dissertation, University of Illinois

at Urbana-Champaign, 2002.

18. Shaffer, C. A., *A Practical Introduction to Data Structures and Algorithm Analysis*, 2nd ed., Prentice Hall, Upper Saddle River, NJ, 2001.
19. Chew, W. C., J.-M. Jin, E. Michielssen, and J. Song, *Fast and Efficient Algorithms in Computational Electromagnetics*, Artech House, Boston, 2001.
20. Bai, L., "An efficient algorithm for finding the minimal loop basis of a graph and its application in computational electromagnetics," M.S. thesis, University of Illinois at Urbana-Champaign, 2000.
21. Keener, J. P., *Principles of Applied Mathematics: Transformation and approximation*, rev. ed., Perseus Books, Advanced Book Program, Cambridge, MA, 2000.
22. Golub, G. H., *Matrix Computations*, Johns Hopkins University Press, Baltimore, 1996.